Microscopy and electron spectroscopic study of the interfacial chemistry in Al–Ti alloy/graphite systems

S. SEAL
Advanced Materials Processing and Analysis Center (AMPAC) and Mechanical, Materials and Aerospace Engineering (MMAE) University of Central Florida, Orlando, FL, USA
E-mail: sseal@pegasus.cc.ucf.edu

T. L. BARR
Department of Materials and Laboratory for Surface Studies, University of Wisconsin-Milwaukee, Milwaukee, WI 53201, USA

N. SOBCZAK
Foundary Research Institute, Krakow, Poland

S. J. KERBER
Material Interface Inc., Sussex, WI 53089, USA

The chemical and physical interaction of liquid metal surfaces with various substrates is an important, largely unexplored aspect of technology, with implications in composite science and catalysis. In the present case, we have employed X-ray photoelectron spectroscopy (XPS) and Auger electron spectroscopy (AES), in conjugation with sessile drop wettability tests, to examine the interfacial properties and surface chemistry of the systems formed by adding liquid drops of select Al–Ti alloys to graphite substrates. A variety of different chemical states was revealed in the XPS results, suggesting the formation of separate regions composed of elemental metals, alloys and carbides. Many of the specific features detected appear to depend on the various treatment properties, e.g. the temperature, bulk alloy composition, size and shape of the alloy drop and time of interaction. The surface analyses were also supported by optical microscopy, scanning electron microscopy (SEM) and X-ray diffraction (XRD) studies. The combined results suggest the induction of a strong reaction between titanium and carbon, resulting in an improvement in the wettability of the alloy with the graphite substrate and a corresponding structure transformation from the ($L_{Al–Ti} + Al_3Ti$) state to the ($L_{Al–Ti} + TiC$) semi-liquid state. © *1998 Kluwer Academic Publishers*

1. Introduction

The interaction of liquid metals with various substrates, such as graphite, plays an important role in the manufacture, treatment and application of numerous materials because of their immediate effect on both the surface and bulk properties of the resulting products [1–4]. The wettability, morphology, and resulting chemical reactions all play central roles in the ability of these systems to achieve their desired physical and chemical properties, and have been the subjects of a number of investigations [5, 6]. The interfacial reactivity, however, still remains an important, largely unexplored question in composite technology.

Ternary Al–Ti–C systems provide various possibilities for practical applications such as: (1) the production of metal matrix composites (MMCs) based on Al/C systems (e.g. when aluminium is metal reinforced by carbon fibres or graphite particles, or when, in a similar system, titanium is used as an active alloying element to obtain better wettability and compatibility between the aluminium matrix and the reinforcing phase) [7–9]; (2) the case of aluminium MMCs reinforced by dispersed TiC particles, particularly using a procedure referred to by metallurgists as the *in situ* technique [10–12]; (3) the production of *in situ* ceramic composites produced by the reactive infiltration technique [13]; (4) cast Al–Ti–C grain refiners of aluminium alloys [14]; and (5) when graphite/graphite or graphite/aluminium are joined through the use of titanium coatings [15]. In the present case, Al–Ti/graphite systems have been formed during wettability testing by the sessile drop method [16].

Because of the importance of the resulting interfaces, it seems appropriate to employ surface analysis techniques to investigate the properties in this evolving region. In the present case, Auger electron spectroscopy (AES) and X-ray photoelectron spectroscopy (XPS) have been employed to examine the resulting

surface and interfacial chemistry. These surfaces analysis techniques analyse the outer 1–8 nm of a material. Generally, in these regions, there will also be some adsorption of and chemical involvement with air-induced species. In this regard, metallic samples are particularly reactive and generally exhibit a significant, if very thin, concentration of native oxides and hydroxides, as well as other adsorbed surfaces species. For example, aluminium metal produce a 20 nm coating of Al_2O_3 in a matter of minutes, even at 10^{-6} torr (1 torr = 133.322 Pa). In addition, adsorbed carbonaceous species (particularly hydrocarbons), designated as adventitious carbon, are always found [17]. On the other hand, these adsorbed oxides and carbonaceous species are relatively inert to more deleterious environmental effects, thus providing a modest form of "natural" passivation. Whatever the case, the nature of these environmental effects [18, 19] may usually be easily recognized and separated from the detected properties of the experimental interfaces of interest herein. Further, the persistent adventitious hydrocarbons often provide a basis for establishing the photoelectron binding energy scale needed for XPS chemical analysis.

2. Experimental procedure
2.1. Materials
Aluminium (99.99%) and its alloy with 10% Ti (designated as AlTi10) were employed in this study. The latter was characterized by a homogeneous distribution of Al_3Ti phases in the aluminium matrix [16]. Before the mixing experiments, K and E28 type graphite substrates (produced by Polgraph Co., Poland, see Table I), were polished to a 0.1 μm finish, cleaned in acetone and annealed in a moderate vacuum at 950 °C. The alloy specimens were also mechanically cleaned on all faces immediately before involvement with the carbon. Table I presents some of the physical characteristics of the K and E28 graphite. The mechanical strength and hardness of the K type graphite is comparatively higher than that of the E-28 type graphite. Two different alloy/graphite systems having the same chemical composition, but different times and temperature treatments (designated herein as Samples 1 and 2) were studied by XPS. In both cases, the alloy was AlTi10 and the graphite substrate was K type. Sample 1 was heated to 950 °C for 60 min, while Sample 2 was heated to 1050 °C for 30 min. In addition, we have studied and compared interfaces of AlTi10 with two different graphite substrates (K and E28 type) heated to 1050 °C for 30 min. The interfaces were diamond cut or laboratory fractured, opened, and analyzed directly. Some additional samples were also analysed by AES as polished cross-sections following investigations with scanning electron microscopy. Additionally, the following reagent-grade reference materials were analysed by the same methods: Al°foil, Al_2O_3 Ti°foil, TiC, TiO_2 graphite, carbon black, and the base alloy AlTi10.

2.2. Spectroscopy
AES [21] analyses were conducted employing a Varian Auger spectrometer. The method is ideal for

TABLE I Physical properties of K and E28 type graphite manufactured under similar conditions

Sample	Density (kg dm^{-3})	Electrical resistivity (μΩm)	Hardness (sh)	Bend strength (MPa)	Compressive strength (MPa)
K	1.00	15.3	49	32.6	60.0
E28	1.69	30.0	42	22.6	32.6

surface elemental qualitative and relative quantitative analysis. Some chemical identifications was also achieved. The base pressure during our Auger study was generally less than 3×10^{-8} torr. The primary voltage of the electron gun was 3 kV and the electron beam current was 10 mA. During depth profiling, a 2 keV Ar$^+$ beam was employed for etching purposes using a source of high-purity argon at a pressure of 5×10^{-6} torr. The electron beam current during these profiles was 25 mA.

X-ray photoelectron spectroscopy (XPS or ESCA) analyses were achieved using a Hewlett Packard (HP 5950A ESCA spectrometer [17, 21], at a base pressure of 2×10^{-9} torr. The AlK$_\alpha$ X-ray system was run at 600 W. Any sample charging was removed with a low-energy electron flood gun. The XPS spot size was 1×5 to 1×1 mm. This XPS system employs an X-ray monochromator to improve energy resolution and sensitivity. Additionally, depth information from these samples was obtained with angular resolved XPS and Ar$^+$ ion etching. The former technique utilized different source/sample geometries, with grazing angle incidence yielding extreme surface information, while increasing the angle increased the depth of analysis. In the present case, the interfaces of Samples 1 and 2 were analysed at angles of 18, 38, and 68°, corresponding to an approximate depth range from 1–8 nm.

3. Results and discussion
3.1. Microscopic analysis of the wettability samples
Fig. 1a, b show the representative microstructure of an Al–Ti10/C (K type) interface, taken after examination of cross-sections of the samples by the sessile drop tests at various temperatures. After testing at temperatures of 950 and 1050 °C, all samples exhibited continuous phases at the alloy/graphite interface. After etching with Kellar's reagent, complicated structures of the interface were detected, revealing the presence of two phases (see Fig. 1). Scanning electron micrographs (Fig. 2a) and the corresponding EDS images (Fig. 2b, c and d, interfacially distributed) of aluminium, titanium and carbon exhibited continuous phases suggesting TiC and $TiAl_2C$ [16, 22], as confirmed by the X-ray studies [16]. The formation of this TiC would appear to be due to the relatively strong reactivity between titanium and carbon. The thickness of this phase, as well as its microstructure, seems to be dependent on the temperature and time of contact. The presence of a TiC phase was also found in the form of fine carbide particles above the interface inside a
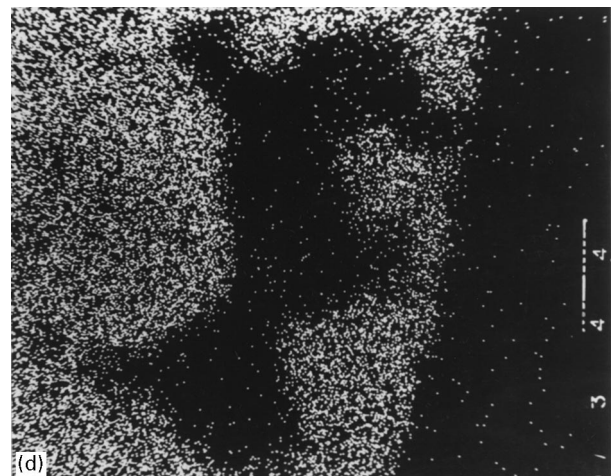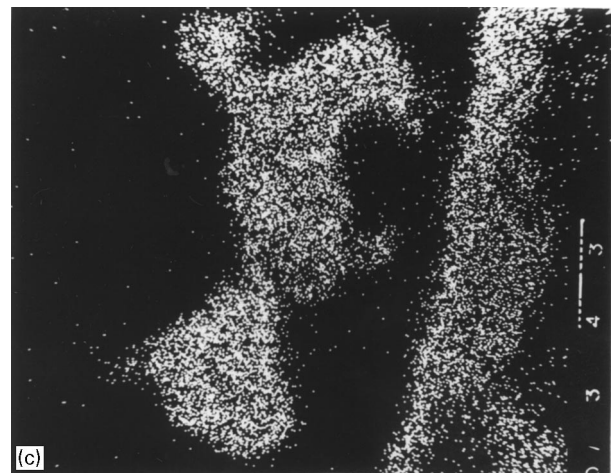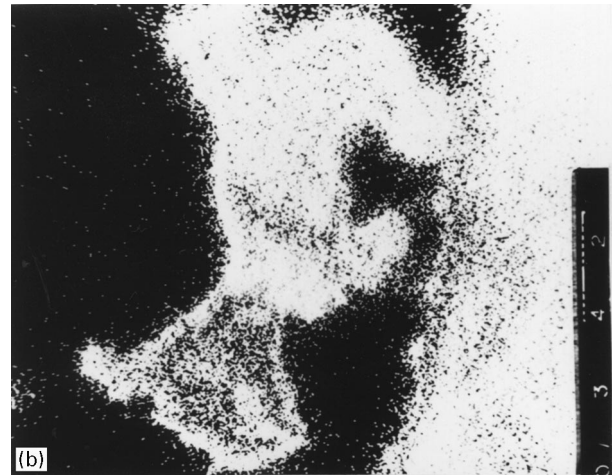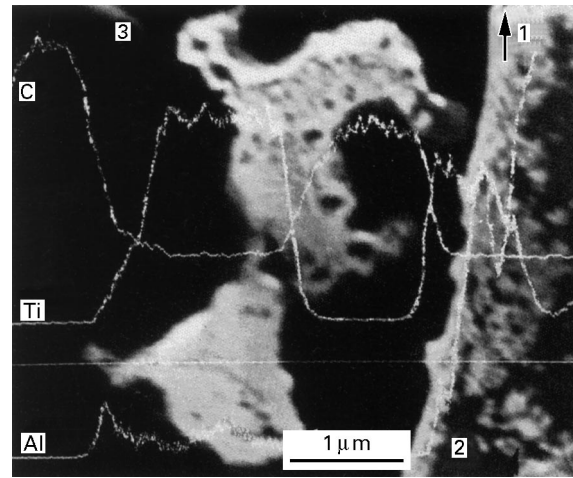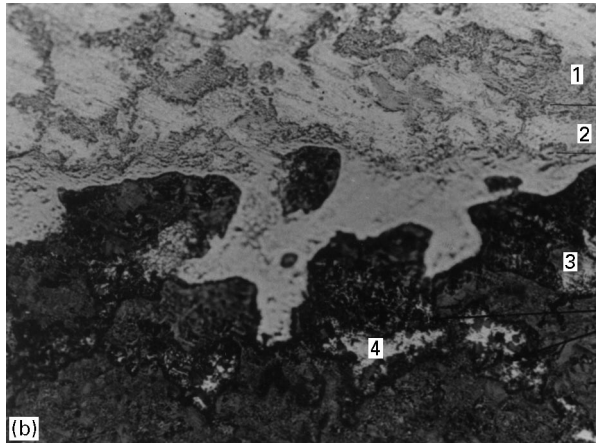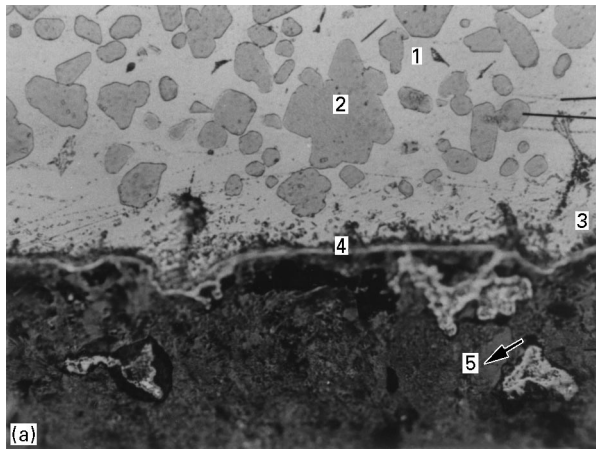
Figure 1 Microstructure (after etching with Kellar's reagent) of the interface boundary between Al–Ti10 alloy and K graphite substrate after wettability testing at (a) 950 °C, 60 min contact, mag × 500 (1) Al, (2) Al_3Ti, (3) TiC, (4) $TiAl_2C$, (5) porous graphite substrate, and (b) 1050 °C and 30 min contact, mag × 500, (1) L_{AL} + TiC, (2) $TiC/TiAl_2C$, (3) porous graphite substrate, (4) Al_4C_3.

region dominated by the alloy (see Fig. 1a). The amount of this phase also seemed to increase with temperature and time of contact. The AlTi10 alloy heated to 1050 °C for 30 min (Fig. 1b) showed more TiC than exhibited by the same alloy heated to 950 °C for 60 min (Fig. 1a). It is suggested that at the present temperature of investigation, the process of interfacial TiC formation simultaneously appears with the solution–reprecipitation process [10].

Due to physico-chemical interaction between alloy and graphite substrate, the phase composition of the drop changes. The formation of solid TiC results in decreased titanium content in the liquid phase (see Fig. 1). This results in the dissolution of some of the Al_3Ti phase in the liquid, which, in turn, makes the total volume of the Al_3Ti phase in the drop less than suggested by the Al–Ti phase diagram [22]. Finally, a structural transformation of the solidifying drop from one semi-liquid state to another apparently is produced, i.e. from $(L_{Al-Ti} + Al_3Ti)$, to $(L_{Al-Ti} + Al_3Ti + TiC)$ (Fig. 1a), or $(L_{Al} + TiC)$ (Fig. 1b).

Figure 2 Scanning electron micrograph with elemental concentration profiles and the corresponding EDS images of (b) aluminium, (c) titanium and (d) carbon of AlTi10/graphite. (1) contact boundary, (2) Al–Ti drop, (3) porous graphite substrate.

It had also been suggested that an improvement in wettability initiates the *in situ* infiltration of Al–Ti alloy into the porous graphite substrate (Fig. 1b). In the case of the K type graphite used for the current experiment, this wettability enhances the formation of the graphite impregnation region [16]. On the other hand, due to the lower strength of graphite E28, (Table I), infiltration of the alloy helps in the local separation of some regions of E28 substrate resulting in erosion of this graphite material [16]. The Al_4C_3 precipitates were apparently observed in the impregnated or eroded regions of both graphites near the drop/substrate contact boundary, with less carbide detected in the case of K-type (Fig. 3a) than E28-type (Fig. 3b) graphite. As described below, a similar result was detected in the XPS results. This result may be explained by the appearance in the interfacial region (between the graphite material and the aluminium alloy) of places where the TiC layer was discontinuous and the titanium concentration in the melt was negligible as a result of TiC formation.

3.2. AES results
Auger (AES) studies have been conducted of a number of the materials of interest in this programme. This includes several of the precursor systems, as well as samples of the solidified AlTi10 alloys and liquid drop implants of the latter on both K and E28 type graphite

Figure 3 Microstructure of (a) AlTi10/K graphite, mag × 500, (1) TiC, Ti_2AlC layer, (2) Al_4C_3, (3) infiltrated region of graphite substrate, (4) contact boundary between the drop and the substrate, and (b) AlTi10/E28 graphite for 30 min treated at 1050 °C, mag × 500, showing the liquid metal infiltration into the graphite substrate, (1) Al, (2) Al_3Ti, (3) mixed carbide layer, (4) infiltration, (5) graphite substrate.

substrates. The results were somewhat disappointing, but not uninformative. First, examinations of several spots on a representative, pretreated AlTi10 alloy revealed the anticipated adventitious carbon and a substantial presence of surface-oriented aluminium, obviously in the alumina state. No elemental aluminium was detected. Sputtering of these samples removed much of the adventitious carbon, but because of the uncontrollably rapid regrowth of Al_2O_3 did little to alter the "proportions" of oxides detected. All of this merely verified what was found in the ESCA analysis, i.e. that air exposure of these alloys, particularly under the thermal conditions involved, results in the growth (on the alloy) of a layering of oxides with at least 2 nm alumina on top of a relatively thin layer of titania.

Similar AES investigations of the AlTi10/graphite systems revealed much of the same presences, with the added proviso that the alumina overlayer was even thicker and a thin, but persistent layer of graphite was apparently drawn over the surface as a result of the sample cleavage. As a result, for these samples the sublayer titania disappeared entirely from (AES) view.

3.3. XPS results
In order to understand the surface chemical reactions between AlTi10 alloy and the graphite (both K and E28 type) substrates, it is necessary to study the surface chemistry of the alloy and the graphites separately.

3.3.1. Surfaces of the graphite systems (K and E28 type)
Table II summarizes the results of the ESCA characterization of the K and E28 graphite before and after temperature treatment at 950 °C for 15 min. The C(1s) binding energy for both types of graphite is in good agreement (284.5 ± 1 eV) with the published literature [23]. Despite the apparent integrity and the generally poor reactivity of graphite, it is well known to suffer from versions of the aforementioned natural passivation [23]. Based on the shoulder on its C(1s) spectrum (see Fig. 4), and O(1s) spectra (not shown), K type graphite seems to have undergone more of this type of oxidation than E28. The oxides formed on the K type appear to represent the presence of a mixture of carbonyl, epoxide and hydroxide bonds, whereas E28 has more air-generated carbonyl types and a lesser presence of epoxides and hydroxides. The C(1s) loss spectra for K graphite also reveals a better resolution
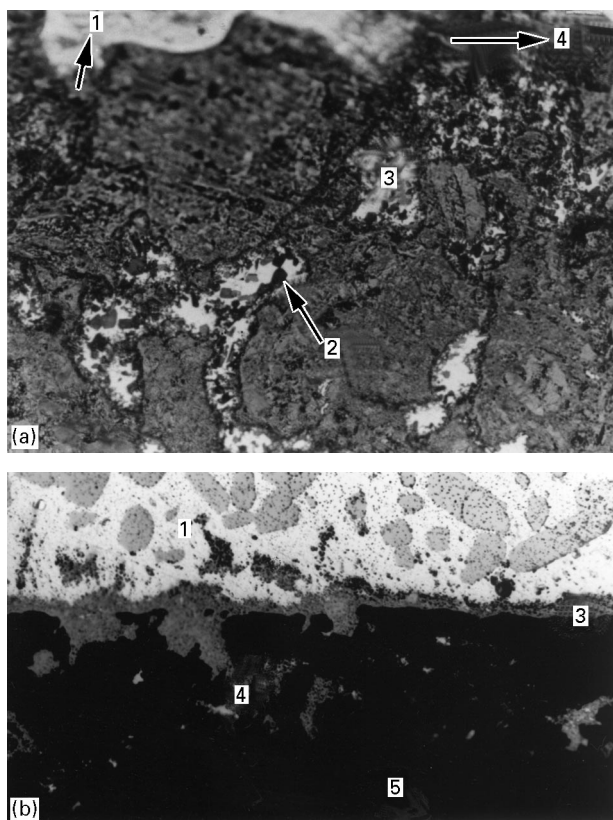
TABLE II XPS results of K and E28 grapite

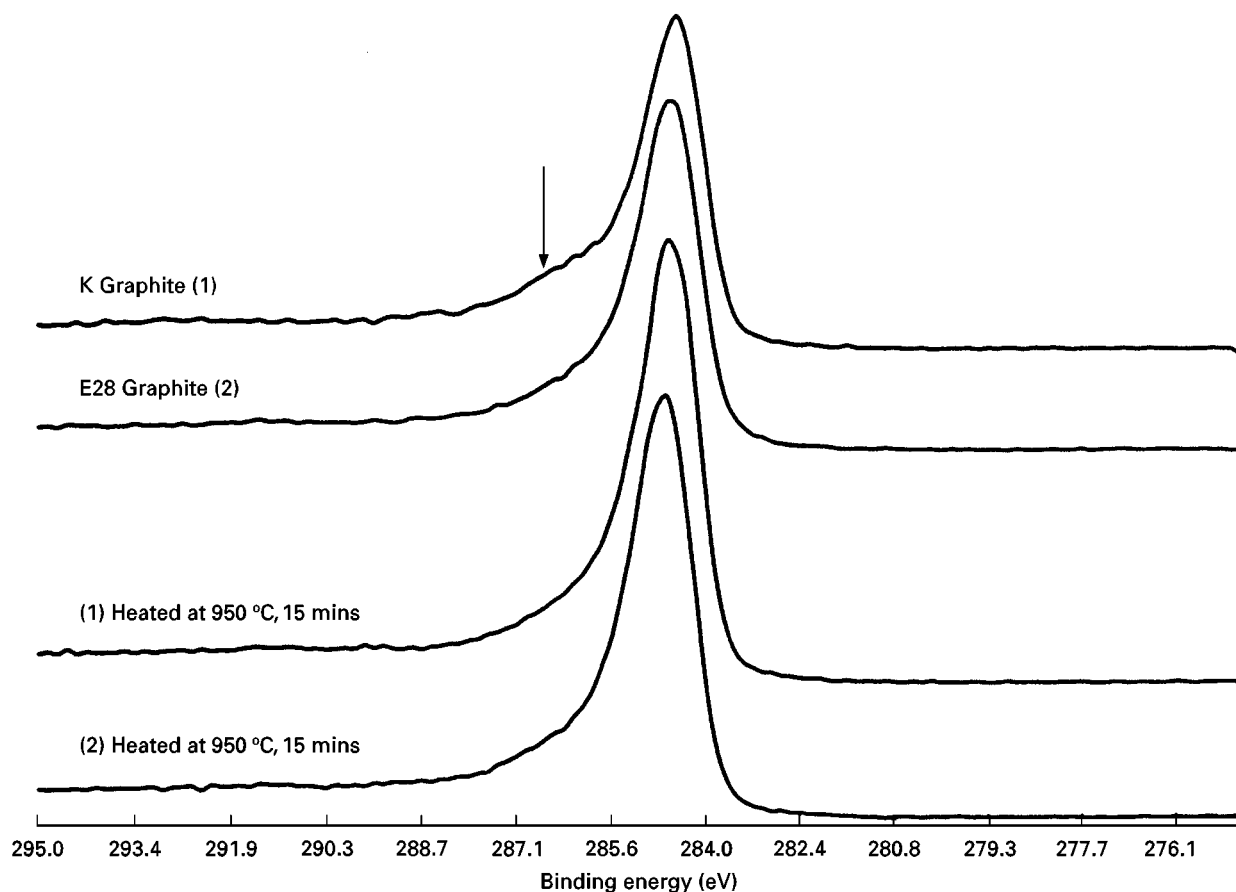| Graphite	C(1s) (eV)	1st C(1s) loss (eV) (*F_{loss})	O(1s) (eV)
K	284.4	29	531.9
E28	284.5	~28–32	531.7
K (heated at 950 °C, 15 min)	284.5	~31.7	532.7
E28 (heated at 950 °C, 15 min)	284.5	~29–32	532.0

Figure 4 C(1s) spectrum for pre- and post-treated (950 °C, 30 min) graphite substrates (K and E28).

of the π–π* transitions (discussed below), than are present in the case of E28. The latter feature relates to the continuous structural integrity of the graphitic (benzene) ring structures [17].

3.3.2. C(1s) loss spectra

Recently, our research group [17] has determined that the position of the relatively weak, broad (plasmon dominated) loss peaks that arises between 20 and 30 eV upfield (the first broad loss splitting) from the C(1s) line, can be used as a means to determine various changes in chemistry for a carbonaceous systems [23]. Thus, we have determined that the loss splitting for true graphite should essentially duplicate that of a free π electron plasmon calculated at 31.0 eV. Variations from this feature may be indications of a reduction in graphitic character, e.g. a typical hydrocarbon loss splitting is ~22 eV [17]. For K graphite we observe a relatively, sharp C(1s) loss peak at ~29–31 eV (Fig. 5a and b) and a moderate second loss peak occurs at ~31–32 eV upfield from the former. From the E28 graphite loss spectra (see Fig. 5c and d), the first loss peak at 28–32 eV is broad and the second peak is practically imperceptible. This second loss line is important because a true (total) plasmon spectrum should exhibit several equally spaced loss peaks, decreasing in size in a regular Poisson distribution. Thus, in the case of a hypothetically perfect graphite, this loss peak character would be a direct reflection of the infinite nature of the conjugated π electron density.
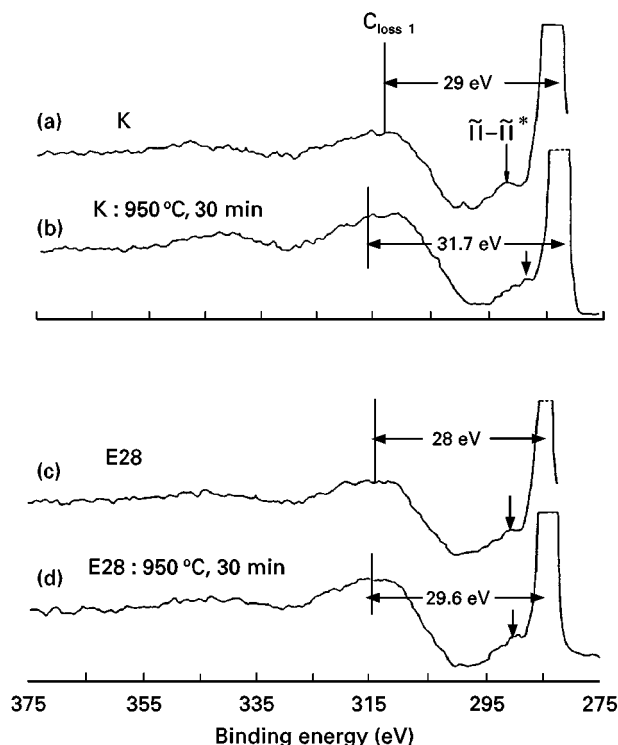

Figure 5 C(1s) loss spectra for both pre- and post-treated graphite substrates (K and E28).

In our case, properly positioned and sized loss peaks are reflections of the presence of relatively good basal plane structures and orientations with few, if any, chemical anomalies. All of this suggests that the K

4151

system is more graphitic than E28. This contention is also consistent with the physical properties listed in Table I. In the case of the heat-treated graphites, the trend in the loss spectra is similar (Fig. 5b and d) to the cases of the unheated ones, except that the first loss peak for both graphite systems occurs at slightly higher binding energy as shown in the Table I.

Thus, in summary, K graphite seems to have both a better ring planar structure and more interconnecting oxides (epoxide and hydroxide) compared to E28. These features may address the relatively poor mechanical strength of E28 compared to K graphite as listed in Table I [24]. On the other hand, it seems that due to the poor mechanical strength of E28 graphite, we observe more infiltration of the liquid alloy into the graphite system for AlTi10/E28 (Fig. 3b), than for AlTi10/K, see Section 3.1.

The binding energy of O(1s) for both the heat-treated K and E28 graphites increases (see Table II) compared to the peak positions for the unheated graphites. There is also a decrease in oxygen content when K and E28 graphites are heated at 950 °C. On heating, the weak C–O–C should break and the corresponding carbonyl group should be removed, thus producing a higher binding energy for the O(1s) lines. Also, in the case of the heated K and E28 graphites, the OH species disappear and the corresponding C(1s) spectrum looks much cleaner (oxide free) than that of the unheated graphites.

3.3.3. XPS results of AlTi10 alloys

The C(1s) peak of the adventitious carbon for an unsputtered AlTi10 alloy is shifted about 1.5 eV upfield (to 286.1 eV) due to charging. The appropriately positioned Al(2P) and Ti(2p) (shifted to reestablish the C(1s) for any C_xH_y at 284.6 eV [28]) are mostly attributed to the presence of the oxides and elemental forms of both metals on the surface (Table III). The Al(2p) reveals the formation of bulk aluminium oxide on the surface of the alloy, as is also evident from the relative Al/O ratio (see Table IV). In the case of sputtered AlTi10 alloy, using a flood gun for charge correction (see Fig. 6), we observe a broad Al(2p) spectrum consisting of several peaks near 74.8 eV and others in the range of 72.8–73.4 eV. The peak structures in the range of 72.8–73.4 eV are apparently indicative of elemental aluminium in either the alloy (Al_3Ti phase as detected by X-ray diffraction) or "detached" Al^0 forms. Following sputtering, the adventitious carbon layer disappears while the most of the

oxides are retained. Also the Al/O ratio decreases and the Al/Ti ratio increases compared to the unsputtered alloy (see Table IV). Although we observe a decrease in the Al/O ratio during sputtering, the Ti/O remains unchanged, suggesting that the surface of the alloy is initially covered with an alumina on the top of the titania layer. In the Al_3Ti phase, the aluminium dominates the oxidation process [13]. The titanium spectrum of the unsputtered AlTi10 alloy is dominated by a $Ti(2p_{1/2})$ peak at 459.5 eV, which is assigned to Ti^{4+} (TiO_2 and $Ti(OH)_4$) on the AlTi system, based on a reference titanium binding energy for TiO_2 at ~ 458.8 eV [21]). All of this suggests the formation of a mixed (Al–Ti–O) oxide. The explanation of the detected higher binding energy of titanium may be due to the peculiarities of the alloy oxide. A small peak at 454.5 eV (Fig. 7) is due to the presence of titanium in the AlTi10 alloy (possibly Al_3Ti), as is evident from the

TABLE IV Relative XPS quantification of AlTi10 alloy

Sputter time (min)	$(Al/Ti)_{oxide}$	AlE/Ti	$(Al/O)_{oxide}$	$(Ti/O)_{oxide}$
0	9.41	3.7	7.26	0.077
30	16.9	9.10	1.29	0.076

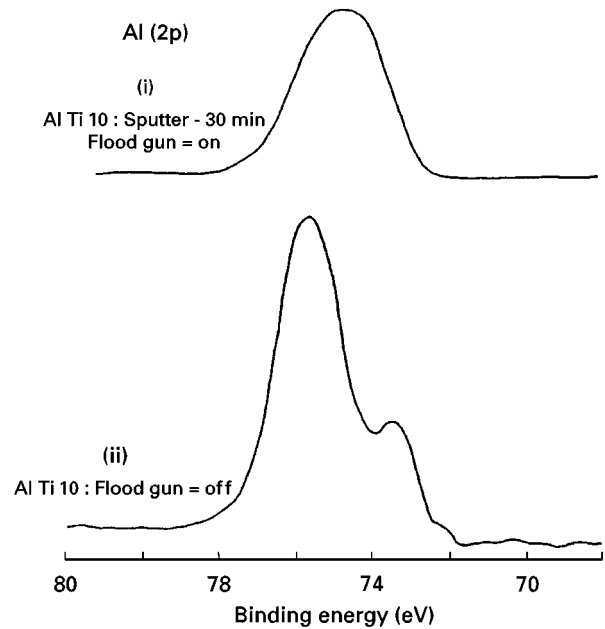*Figure 6* (a) Al(2p) spectra of AlTi10 alloy: (i) sputtered for 30 min, flood gun on, (ii) unsputtered, flood gun off.

TABLE III Binding energy results of AlTi10 alloy

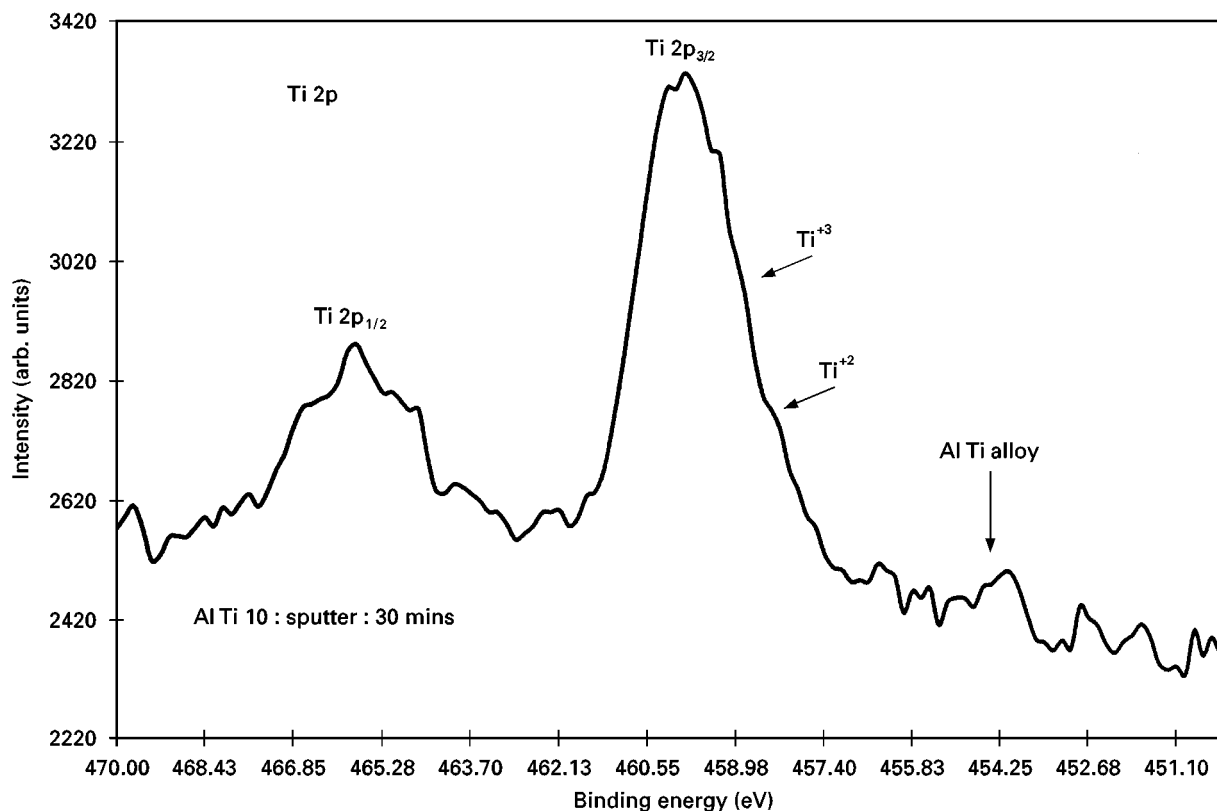| Sputter (min)	Flood gun	C(1s) (eV)	O(1s) (eV)		Al(2p) (eV)		Ti(2p) (eV)	
			Al_2O_3	TiO_2	Al_2O_3	$Al_3Ti + Al^0$	Ti in AlTi alloy	Ti in oxide and hydroxide
0	Off	286.1	533.12	531.2	75.7	73.5–72.8	454.5	459.5
30	On	284.7	531.4		74.8	73.47–73	454.5	459.8

Figure 7 Ti(2p) spectra of sputtered AlTi10 alloy.

X-ray [16] and SEM analysis; pure Ti^0, on the other hand, produces a Ti($2p_{3/2}$), binding energy at 454.1 eV. Also, the O(1s) spectrum is broad and multi-peaked revealing the presence of peaks related to Al_2O_3 (531.7 eV [21]) and TiO_2(529.7 eV [21]), respectively. Note that we have also included a few "flood gun off–flood gun on" results. Perhaps the most significant feature of these is that the latter substantially effects the position of the significant charging Al_2O_3 peaks (Fig. 6a and b), but not the slightly charging TiO_2.

3.3.4. XPS results for AlTi10 alloy/graphite (K and E28) systems

The original C(1s) peaks for the interfaces of the AlTi10 alloy interacted with K and E28 graphites (heated to 1050 °C for 30 min), appeared at 286.1 and 286.3 eV, respectively, thus suggesting a charging produced by the adventitious carbon and insulating oxides formed at the outer surface of the investigated alloy/graphite interface, i.e. the graphite substrate was not detected. The outer surface oxidation of the AlTi alloy component when mixed with the K graphite is larger than that for the alloy interacted with E28 graphite as is evident from these C(1s) spectra (not shown). This clearly indicates the differences in the interfacial reactions of the alloy with the different graphite substrates despite their similar treatments. This result is supported by the behaviour of the aforementioned carbon XPS results for the pre-interacted K and E28 graphite systems described in Section 3.1.

In the O(1s) binding energy region, the oxygen produces two charge-corrected peaks in the AlTi10 alloy/ graphite (K and E28) system. The peak with the lower binding energy seems to suggest primarily O(1s) for Al_2O_3 with a typical value of 531.8 ± 0.1 eV, whereas the binding energy shoulder peak is that due to $Al(OH)_3$ (533.4 eV). Based on the comparative peak size analysis, we found that the intensity of the oxygen peak is higher in the AlTi10/graphite(K) compared to AlTi10/graphite(E28). The O(1s) peak structure apparently results from the aluminium oxygen interaction.

In the case of titanium, the charge-corrected binding energies of Ti $2p_{1/2}$ and Ti $2p_{3/2}$ were observed to be at 465 and 459.5 + 0.2 eV for all AlTi10 alloy/ graphite (K and E28) systems (Fig. 8). The peaks at 459 ± 0.2, 458.4 ± 0.2, 457 eV indicate the mixed presence of TiO_2 (Ti^{4+}), Ti_2O_3 (Ti^{3+}) and TiO (Ti^{2+}). The small peaks in the range of 455.5–455 eV suggest the formation of TiC, and possibly Ti_2AlC, at the interface of the AlTi alloy and the graphite substrate, which is also suggested by the microscopic and X-ray analysis of the interface [16]. The titanium concentration, as observed from the relative intensity of the peaks, is several times lower in the case of the AlTi10 alloy/E28 graphite system compared to the alloy interacting with the K type graphite. This may be explained by the interfacial reaction between the E28 graphite material and the alloy, which may occur in places where the titanium carbide layer is discontinuous and the titanium concentration in the melt is negligible, due to the process of TiC formation. The apparent peaks between 454.5 and 454 eV seem to indicate the
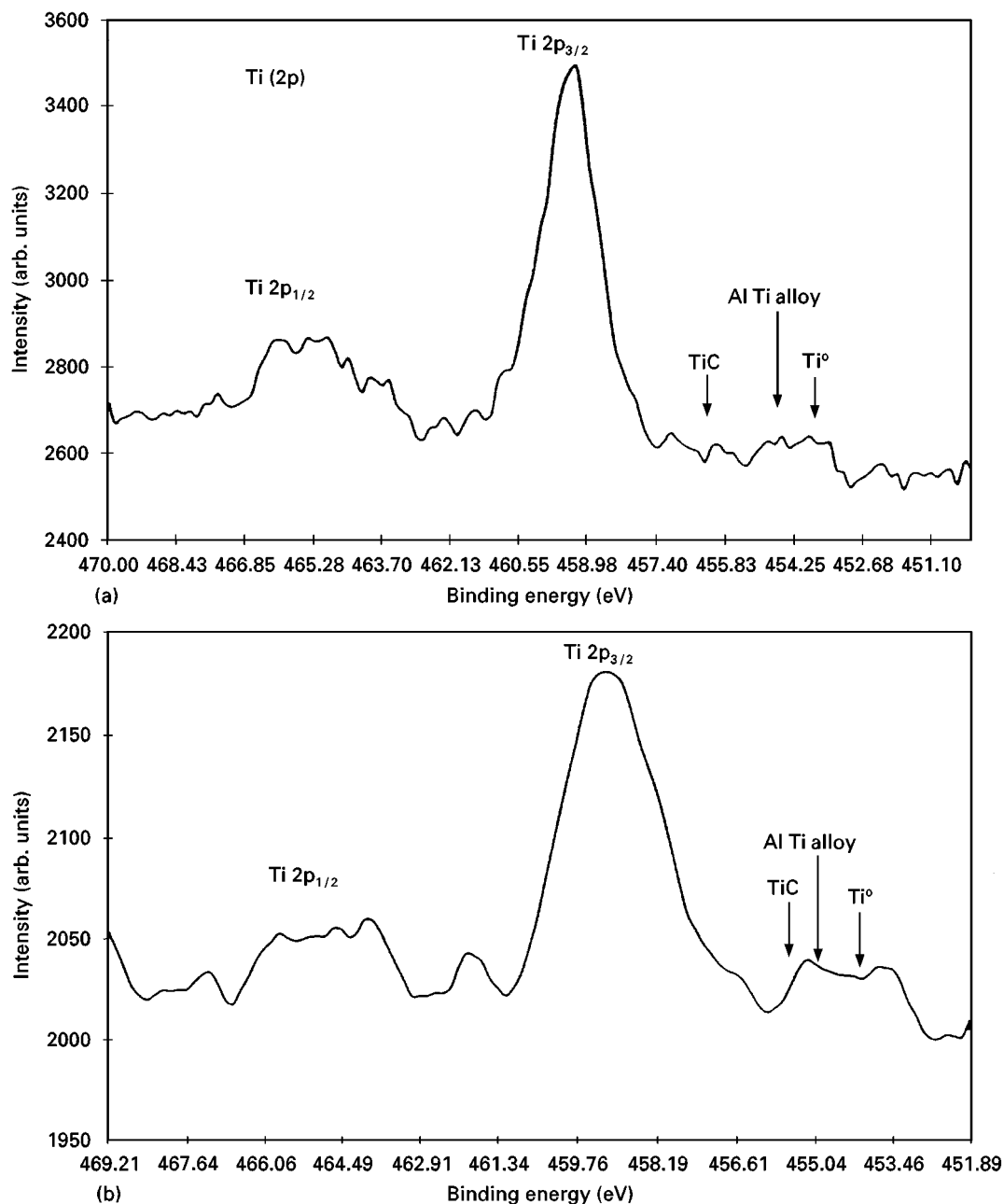
Figure 8 Ti(2p) spectra for (a) AlTi10/C(K), and (b) AlTi10/C(E28).

presence of non-oxidized titanium with the higher binding energy state probably indicative of the titanium in Al_3Ti (see below). The indications of peak structures above 455 eV should be due to TiC. The formation of TiC was also evident from the microscopic analysis discussed earlier suggesting the strong chemical interaction between the titanium in the alloy and the graphite substrate.

In the case of aluminium, the removal of charging results in substantial overlapping of the oxidized and elemental Al(2p) peaks. (The larger splitting in the case of the non-charge-corrected result occurs because up-field charge shifting only occurs for the insulating Al_2O_3 [17].) We are still able to identify Al(2p) for Al_2O_3 (or the hydroxylated form, Table V) at $\sim 75.6 \pm 0.1$ eV consistent with the aforementioned O(1s) peak positions. Similarly, a shoulder peak at ~ 73.3–72.6 eV is no doubt indicative of non-oxidized aluminium, but the X-ray and EDS results suggested that this broad peak should be due to some type of mixture of non-oxidized aluminium in Al_3Ti and Al^0 with the higher binding energy indicative of the latter. Electronic structure considerations suggests that the alloy Al_3Ti should result in a moderate transfer of electron density from the titanium to aluminium [25] i.e. producing a negative binding energy shift. However, because the total of this effect is reduced in the Al_3Ti by 1/3 per aluminium, one should not expect a substantial negative shift in Al(2p) for the transformations of Al^0 to Al_3Ti, and this is consistent with the existing literature data [26]. In order to eliminate the formation of any Al_4C_3 we have also examined the Al(2p) spectra (Fig. 9) with flood gun off to "open up" the separation between the spectra for the charging oxidized aluminium and the non-charging elemental peak. The results here are somewhat ambiguous, but angle-resolved XPS analysis was performed, and in the latter evidence of Al_4C_3 was detected (see below).

TABLE V Binding energy values as obtained from the XPS analysis of AlTi10/C (K and E28), heated at 1050 °C for 30 min

	C(1s) (eV)	O(1s) (eV)	Al(2p) (eV)			Ti(2p) (eV)				Relative Al/Ti
			$Al(OH)_3$	Al_2O_3	$Al_3Ti + Al^0$	$Ti(OH)_4$	TiO_2	TiC	$TiAl_3 + Ti^0$	
AlTi10 C(K)	284.5	531.9	75.7	74.6	73.3–72.6	459.4	458.7	455.2	454.8–454.1	17
AlTi10 C(E28)	284.4	531.7	75.6	74.4	73.3–72.53	459.2	458.3	455.4	454.5–454	24
TiC	281.7		–	–	–			455.5		–

Note: Those who wish to see tabulation from independent sources with comparable peak identification (as shown in Tables I–V), consult [2].
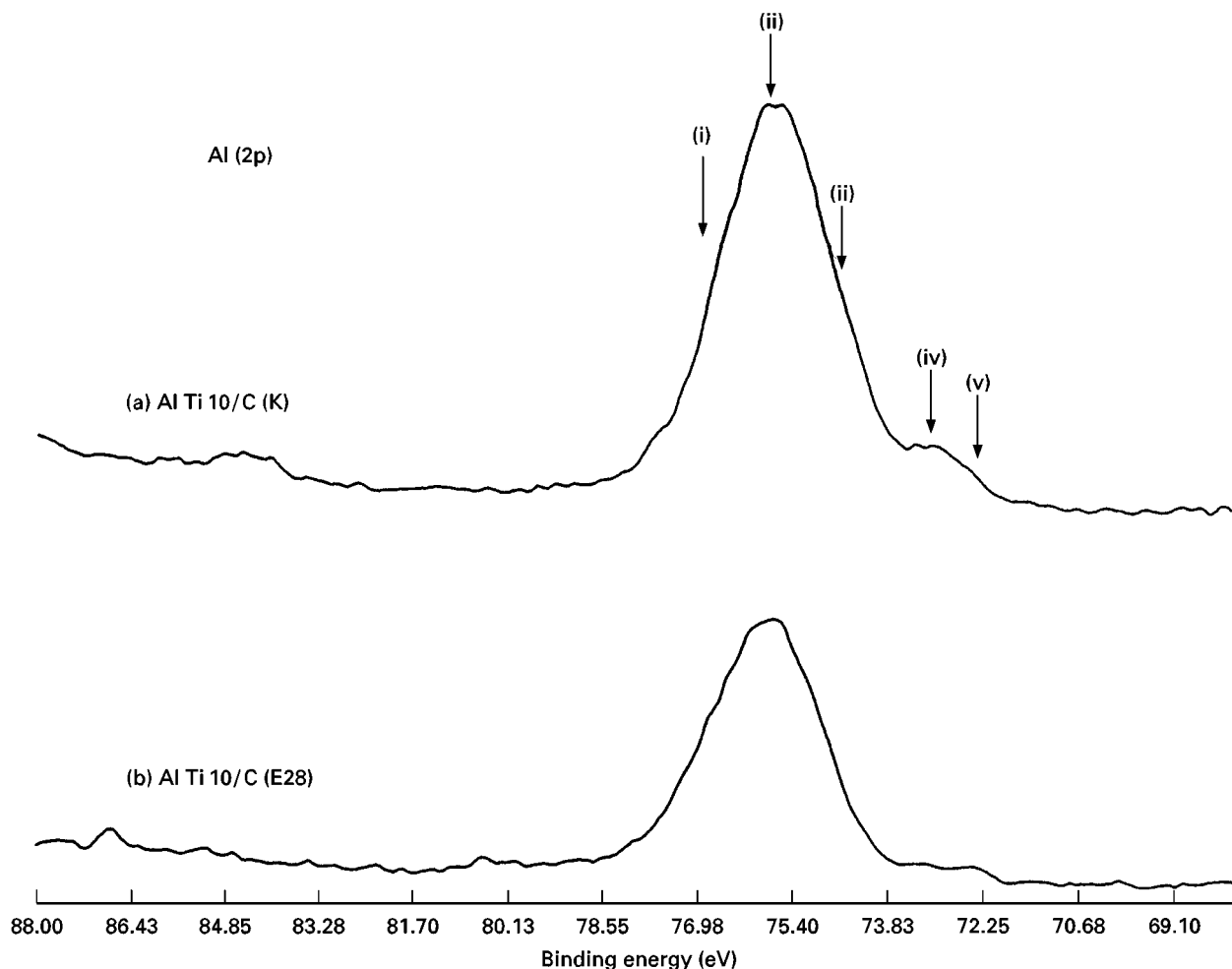

Figure 9 Al(2p) spectra for (a) AlTi10/C(K), and (b) AlTi10/C(E28) (i) $Al(OH)_3$, (ii) Al_2O_3, (iii) Al_4C_3, (iv) Al^0, and (v) Al_3Ti.

3.3.5. Angle-resolved XPS results

XPS analyses were also conducted in the angular resolution mode of several samples as outlined earlier. Grazing incidence (18°) analysis of a polished cross-section of the interfacial area of a sample, designated Sample 1, revealed a broad, multipeaked C 1s peak signal, suggesting the detection of macroscopic structural flaws on the surface indicative of several different types of carbonaceous species, apparently representative of the carbon in each major flaw area. The analysis spot mandates (in this case) that the carbon photoelectrons were simultaneously detected from a somewhat receded metallic surface and a slightly raised graphite surface, as well as from the interface [27]. This ensures that apart from the detected surface is off the Rowland circle and therefore not in focus. In the present case, this disparity causes both a slight peak broadening and shifting [17]. Thus, the C1s peak for the adventitious carbon adsorbed on the now out of focus aluminium (Fig. 10a) is down-shifted about 1 eV (to 283.4 eV) from that for the focused graphite (at 284.4 eV, Fig. 10b) [28]. The resulting Al 2p-produced linewidth for Al_2O_3 was 1.6 eV (see Fig. 10a). This is indicative of a singular (Al_2O_3-only) peak devoid of any of the mixed chemical (or morphological) species that were found to be present in the carbon, but as in the case of the (covering) adventitious carbon, this Al(2p) peak was shifted down-field 1 eV (to 74.6 eV) because of the recessed (non-XPS focussed) surface of the metal side in our analysis. Additionally, there was
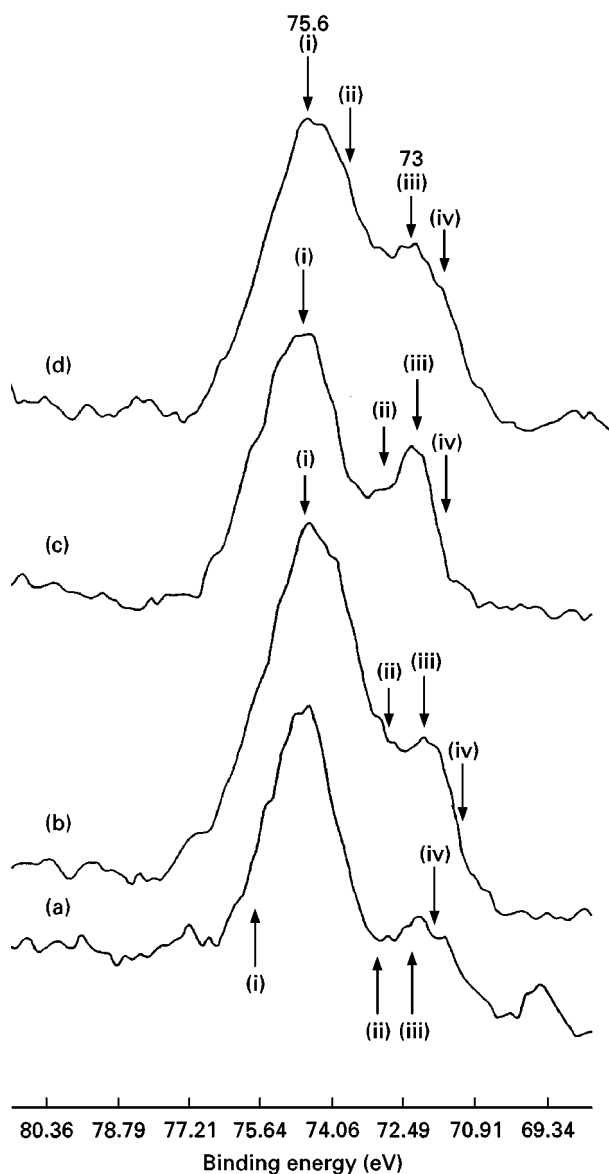
4155

75.6
(i)

(ii)

73
(iii)

(iv)

(d)

(i)

(iii)

(ii)

(iv)

(c)

(i)

(ii) (iii)

(iv)

(b)

(iv)

(a)

(i)

(ii) (iii)

| 80.36 | 78.79 | 77.21 | 75.64 | 74.06 | 72.49 | 70.91 | 69.34 |

Binding energy (eV)

Figure 10 Representative Al(2p) XPS spectra of the Al–Ti/C (graphite) systems described in this study. (a) Near grazing incidence (18°) result for Sample 1. Note that all peaks are offset shifted $\sim 1.0\,eV$ downfield from their conventional position. (i) Singular peak for Al_2O_3, (ii) largely non-existent peak position for Al_4C_3, (iii) peak for elemental aluminium, (iv) Al(2p) peak position for Al–Ti alloy; (b) peak system for Sample 1 at deep incidence 68° ($\sim 8\,nm$), (i) note line broadening of Al_2O_3 peak due to reduced resolution, (ii) Al_4C_3, (iii) Al^0, (iv) note missing Al–Ti peak; (c) aluminium peak structures for sample 2 at 38° (note the Fermi edge shift), (i) Al_2O_3, (ii) Al_4C_3, (iii) Al^0, (iv) lack of Al–Ti alloy; (d) aluminium peaks for sample 2 at 68° deep incidence; (i) Al_2O_3 (note breadth – (lack of resolution?), (ii) Al_4C_3, (iii) Al^0, (iv) Al–Ti alloy, i.e. titanium beginning to "reappear".

a relatively deep valley between the oxidized aluminium peak (74.6 eV, corrected to 75.6 eV [29]) and the metallic peak (72.0 eV corrected to 73.0 eV), suggesting that little or no outer surface Al_4O_3 is being detected. There was also a somewhat small, but reasonably well-resolved shoulder peak at 71.4 eV. This peak, when corrected to 72.4 eV, perhaps suggests the presence of the bimetallic alloy with aluminium as the matrix (e.g. Al_3Ti), which was also found in the microstructural investigations. This downfield binding energy shift is consistent with the presence of Al–Ti alloys, where valence electron density is extracted

from the "d" band of the titanium into the aluminium "p" band, thus making the binding energies of the alloyed aluminium system more negative. The lack of detection of aluminium formation was expected at grazing incidence measurement, because such species should be restricted to the interface region. This was also consistent with the fact that little or no titanium was detected in this region, as was also observed by electron microscopy [16].

Deeper analysis of Sample 1 (at 38°) reproduced many of the aforementioned features, with some important additional information about the interface itself. Thus, the Al 2p peak was now found to exhibit some Al_4C_3 structure [30] and the corresponding Ti(2p) indicated that some titanium, primarily TiO_2, was also detected. The formation of Al_4C_3 occurs due to the infiltration of the liquid aluminium into the graphite substrate. Analysis at 68° proved consistent with this apparent trend by exhibiting a definite growth in Al_4C_3 peak. No aluminium alloy peaks were detected (see Fig. 10b), along with more TiO_2, plus some additional, hard to interpret features, apparently due to reduced titanium species.

On the other hand, Sample 2 was prepared by fracturing along the interface. It was cleaned and then subsequently analysed along its newly exposed surfaces. It was anticipated that the metals side would fracture near materials induced at the interface imperfections (e.g. in the region of any carbides that may be formed). In order to verify this assumption, the resulting surface was analysed with angle-resolved XPS at 38° and 68° angles of incidence.

The initial feature to note in the 38° analysis of Sample 2 was that light cleaning removed most of the visible graphite, but the retained C(1s) spectrum was still predominantly that for a relatively pure graphite with a singular morphology, e.g. no significant adventitious carbon was formed. Lack of coupling of the Fermi edge of this sample caused charging and floating of the C(1s) binding energy downfield by 0.8 eV (to 283.8 eV). This feature was also "tracked" by following the binding energies of the aluminium species, where the oxide Al(2p) was found at 74.9 eV (Fig. 10c) (instead of 75.7 eV) and the Al^0 peak was detected at 72.2 eV (instead of 73.0 eV). There was also an obvious peak structure near 72.8 eV (corrected to 73.6 eV) where the Al(2p) of Al_4C_3 forms, and several other peaks that indicate other aluminium species suggesting the possible formation of mixed alloy carbides. The higher the temperature and time of contact, apparently the higher the probability of Al_4C_3 phase formation. In this case, the probable Al–Ti alloy peak (at 72.5 eV) was missing, perhaps suggesting that such metallic (Al^0–Ti^0) alloys were uncommon at the interface, or that (as mentioned above) a shift of this size is not achieved. Attempts to detect the titanium in this region proved futile, suggesting that titanium was concentrating away from this region of detection. This suggests that the titanium is consumed totally at the interface to form TiC.

The preceding analysis was followed by an attempt to detect features below the outer surface of the metallic interface of Sample 2. This was accomplished by

4156

deeper angular resolution (68°). Interestingly, this reproduced the previously described broadening of the C(1s) line and although some broadening was anticipated in operating the HP spectrometer at 68°, the resulting features seemed to resemble very closely those due to our previously described morphology distortions. In this case, however, the aluminium spectra seem to track the totality of the carbon behaviour, e.g. Fig. 10d. Thus, there is a peak above 75 eV (the conventional Al_2O_3 binding energy), plus an oxidized shoulder shifted to ~ 74.6 eV. Some carbide structure was seen at 73.5 eV, plus the usual Al^0 at 73 eV. The low binding energy shoulder near 72.5 eV may be due to the alloy formation. In the case of titanium, the possible Ti(3d) peak structure near 454 eV seems to indicate the slight presence of the $Ti(3d_{5/2})$, of Ti^0, or TiC, or AlTi alloy. From these peak positions and shapes one can therefore conclude that the interface is very heterogeneous.

4. Conclusions

1. The sessile drop method and subsequent microscopic analysis were found to be useful for studies of the physico-chemical interaction in the Al–Ti–graphite system, when the Al–Ti alloy is in a semi-liquid state. As a result of strong reactivity between titanium and carbon, an improvement in the wettability in the Al–Ti/C system was suggested by the above results and a structural transformation was found from one semi-liquid state ($L_{Al-Ti} + Al_3Ti$) to another; either ($L_{Al-Ti} + Al_3Ti + TiC$) or ($L_{Al} + TiC$) was also indicated.

2. The resulting wettability phenomena indicated the *in situ* reactive infiltration of the alloy into the porous graphite substrate, and the formation of different structures (e.g. (Al–TiC–AlTi$_2$C–C) or (Al–TiC–Al$_4$C$_3$–C) depending on temperature and time of contact.

3. AES and XPS were used to analyse several samples in a study of the interfaces and surfaces formed by the precursor AlTi alloys and graphite system, with particular emphasis on the detection of all chemical species.

4. Auger analysis demonstrated the general lack of cleanliness of the surfaces of these systems, thus reflecting the persistent presence of environmentally induced effects in these types of systems, particularly during the complex physical treatments described here.

5. XPS analysis suggested that K graphite had better structural integrity than the E28 form.

6. Following the wetting experiments, XPS analysis also demonstrated the presence of Al$_3$Ti, TiC and various oxides of aluminium and titanium at the interface of the graphite and the alloy. The XPS results suggested differences in the reaction kinetics of the AlTi10 alloy with the various graphite substrates (K and E28).

7. XPS analysis of the interfaces indicated that aluminium carbide was produced, along with the expected (air-induced) Al$_2$O$_3$ and TiC [31]. Angular resolution studies suggested that these carbides were predominantly located at, or near, the interface. Evidence was also presented for the variable presence of Al–Ti alloys; however, due to the dominating outer surface nature of the oxides, significant levels of titanium, other than TiO$_2$, were not detected in the (as-prepared) interfaces. Angular-resolved XPS proved to be a particularly valuable technique to analyse the chemistry present as a function of distance from the interface.

8. It was pointed out in both the AES and XPS that proper reading of the adventitious carbon and native oxides on the raw materials used in this type of study must be included in any detailed interpretation of the interfacial properties.

9. Another general feature indicated by this analysis is that although both AES and XPS are generally considered as "surface" analysis tools, in the case of the two systems employed in the present study, they are not equal in their depth of analysis into the subsurface, with the HP ESCA apparently capable of deeper investigations than the AES.

References

1. YU. V. NAIDICH, in "Progress in Surface and Membrane Science", edited by J. F. Danielli, Vol. 14 (Academic Press, London, 1981) p. 353.
2. N. EUSTATHOPOULOS, D. CHATAIN and R. SANGIORGI, in "Proceedings of the European Colloquium on Designing Interfaces: Ceramic-Ceramic, Ceramic-Metal Joining", Patent (the Netherlands), edited by S. D. Peteves (Elsevier Applied Science, 1989) p. 197.
3. M. G. NICOLAS, *Proc. Mater. Sci. Forum* **29** (1988) 127.
4. N. EUSTATHOPOULOS, *Int. Metals Rev.* **28** (1983) 189.
5. A. MORTENSON, *Mater. Sci. Eng.* **A135** (1991) 1.
6. YU. V. NAIDICH and G. A. KOLESNICHENKO, "Interaction of Metallic Solutions with diamond and Graphite Surfaces" (Science Publishers, Kiev, 1967) 89.
7. K. YOSHINOBU, Y. MISHIMA, S. UMEKANA and T. SUZUKI, *J. Mater. Sci.* **19** (1984) 107.
8. W. JIANXIN, L. PENGEING, G. MINGYUAN and W. RENJIL, *Compos. Interfaces* **1** (1993) 75.
9. A. N. VARENKOV et al., in "Proceedings of the Moscow International Composite Conference" (Elsevier Applied Science, 1990) 412.
10. A. BANERJI and W. REIF, *Metall. Trans.* **17A** (1986) 2127.
11. A. JARFORS, H. FREDRIKSON and L. FROYEN, *Mater. Sci. Eng.* **A135** (1991) 119.
12. V. SHTESSEL, S. SAMPATH and M. KOCZAK, in "Proceedings of the Symposium on in situ Composites, Science and Technology", 17–21 October 1993, Pittsburgh, PA, pp. 37.
13. S. KHATTRI, V. SHTESSEL, M. KOCZAK, A. P. DIVECHA and J. KERR, *ibid.* p. 115.
14. A. CIBULA, *J. Inst. Metals* **76** (1949–50) 321.
15. C. R. MANNING and T. B. GURGANUS, *J. Am. Ceram. Sci.* **52** (1969) 115.
16. N. SOBCZAK, Z. GORNY, P. K. ROHATGI, M. KSIAZEK and W. RADZIWILL, in "Proceedings Cast Composites", Zakopane, Poland, October 1995, p. 65.
17. T. L. BARR, "Modern ESCA" (CRC Press, Boca Raton, FL, 1994).
18. N. CABRERA and N. F. MOTT, *Rep. Prog. Phys.* **12** (1948) 163.
19. F. P. FEHLNER, "Low Temperature Oxidation" (Wiley, New York, 1986).
20. N. SOBCZAK, *Transaction of Fountry Research Institute*, *XLIV*, **739** (1994) 221.
21. D. BRIGGS and M. P. SEAH, "Practical Surface Analysis", 2nd Edn. (Wiley, Chichester, UK, 1990).
22. A. JARFORS and H. FREDRIKSON, *Microgravity Sci. Technol* **III(4)** (1991) 216.

23. T. L. BARR and M. YIN, *J. Vac. Sci. Technol.* **A10** (1992) 2788.
24. N. SOBCZAK, Z. GORNY, H. KSIAZEK, W. RADZIWILL, P. ROHATGI, in "Proc. Fifth International Conference on Al-alloys." (ICAA-5), July 1–5, 1996, Grenoble, France.
25. S. LIU, R. HU and C. WANG, *J. Appl. Phys.* **74(5)** (1993) 3204.
26. D. E. MERCER, T. R. HESS, T. MEBRAHTU, D. L. COCKE and D. G. NAUGLE, *J. Vac. Sci. Technol.* **A 9** (1991) 1610.
27. P. K. ROHATGI, Y. LIU and T. L. BARR, *Metall. Trans.* **22A** (1991) 1435.
28. T. L. BARR and SEAL, *J. Vac. Sci. Technol.* **A 13** (1995) 1239.
29. T. L. BARR, S. SEAL, LE ME CHEIN and C. C. KAO, *Thin Solid Films* **253** (1994) 277.
30. A. E. HUGES, M. M. HEDGES and B. A. SEXTON, *J. Mater. Sci.* **25** (1990) 4856.
31. N. SOBCZAK, S. SEAL, S. J. KERBER, S. HARDCASTLE, P. K. ROHATGI and T. L. BARR, in "Proceedings of the Cast Composites Conference", Zakopane, Poland, October 1995, p. 38.